nature methods

Resource

https://doi.org/10.1038/s41592-023-02144-y

scPerturb: harmonized single-cell perturbation data

Received: 28 January 2023

Accepted: 4 December 2023

Published online: 26 January 2024

Check for updates

Stefan Peidli[1,2,11] ✉, Tessa D. Green[3,11], Ciyue Shen[4,5,6], Torsten Gross[7], Joseph Min[3], Samuele Garda[2,8], Bo Yuan[4,5,6], Linus J. Schumacher[9], Jake P. Taylor-King[7], Debora S. Marks[3,6], Augustin Luna[4,5,6,10] ✉, Nils Blüthgen[1,2,12] ✉ & Chris Sander[4,5,6,12] ✉

Analysis across a growing number of single-cell perturbation datasets is hampered by poor data interoperability. To facilitate development and benchmarking of computational methods, we collect a set of 44 publicly available single-cell perturbation–response datasets with molecular readouts, including transcriptomics, proteomics and epigenomics. We apply uniform quality control pipelines and harmonize feature annotations. The resulting information resource, scPerturb, enables development and testing of computational methods, and facilitates comparison and integration across datasets. We describe energy statistics (E-statistics) for quantification of perturbation effects and significance testing, and demonstrate E-distance as a general distance measure between sets of single-cell expression profiles. We illustrate the application of E-statistics for quantifying similarity and efficacy of perturbations. The perturbation–response datasets and E-statistics computation software are publicly available at scperturb.org. This work provides an information resource for researchers working with single-cell perturbation data and recommendations for experimental design, including optimal cell counts and read depth.

Perturbation experiments probe the response of cells or cellular systems to changes in conditions. These changes traditionally acted equally on all cells in a laboratory experiment by, for example, modifying temperature or adding drugs. Nowadays, with advanced functional genomics techniques, single-cell genetic perturbations acting on individual cellular components are available. Perturbations using different technologies target different layers of the hierarchy of protein production (Fig. 1). At the lowest layer, CRISPR-cas9 acts directly on the genome, using insertion–deletion polymorphisms to induce frameshift mutations that effectively knock out one or multiple specified genes[1–3]. Newer CRISPRi and CRISPRa technologies inhibit or activate transcription, respectively[4]. CRISPR-cas13 acts on the next layer in the hierarchy of protein production to promote RNA degradation[5]. Small molecule drugs, in contrast, typically act directly on protein products such as enzymes and receptors. When these techniques are applied to large-scale screens they create a map between genotype,

[1]Institute of Pathology, Charité – Universitätsmedizin Berlin, Corporate Member of Freie Universität Berlin and Humboldt-Universität, Berlin, Germany. [2]Institute of Biology, Humboldt-Universität, Berlin, Germany. [3]Department of Systems Biology, Harvard Medical School, Boston, MA, USA. [4]Departments of Cell Biology and Systems Biology, Harvard Medical School, Boston, MA, USA. [5]Department of Data Sciences, Dana-Farber Cancer Institute, Boston, MA, USA. [6]Broad Institute, Cambridge, MA, USA. [7]Relation Therapeutics, London, UK. [8]Institute for Computer Science, Humboldt-Universität zu Berlin, Berlin, Germany. [9]Centre for Regenerative Medicine, University of Edinburgh, Edinburgh, UK. [10]Computational Biology Branch, National Library of Medicine and Developmental Therapeutics Branch, National Cancer Institute, Bethesda, MD, USA. [11]These authors contributed equally: Stefan Peidli, Tessa D. Green. [12]These authors jointly supervised this work: Nils Blüthgen, Chris Sander. ✉e-mail: stefan.peidli@embl.de; augustin@nih.gov; nils.bluethgen@charite.de; sander.research@gmail.com

https://doi.org/10.1038/s41592-023-02144-y

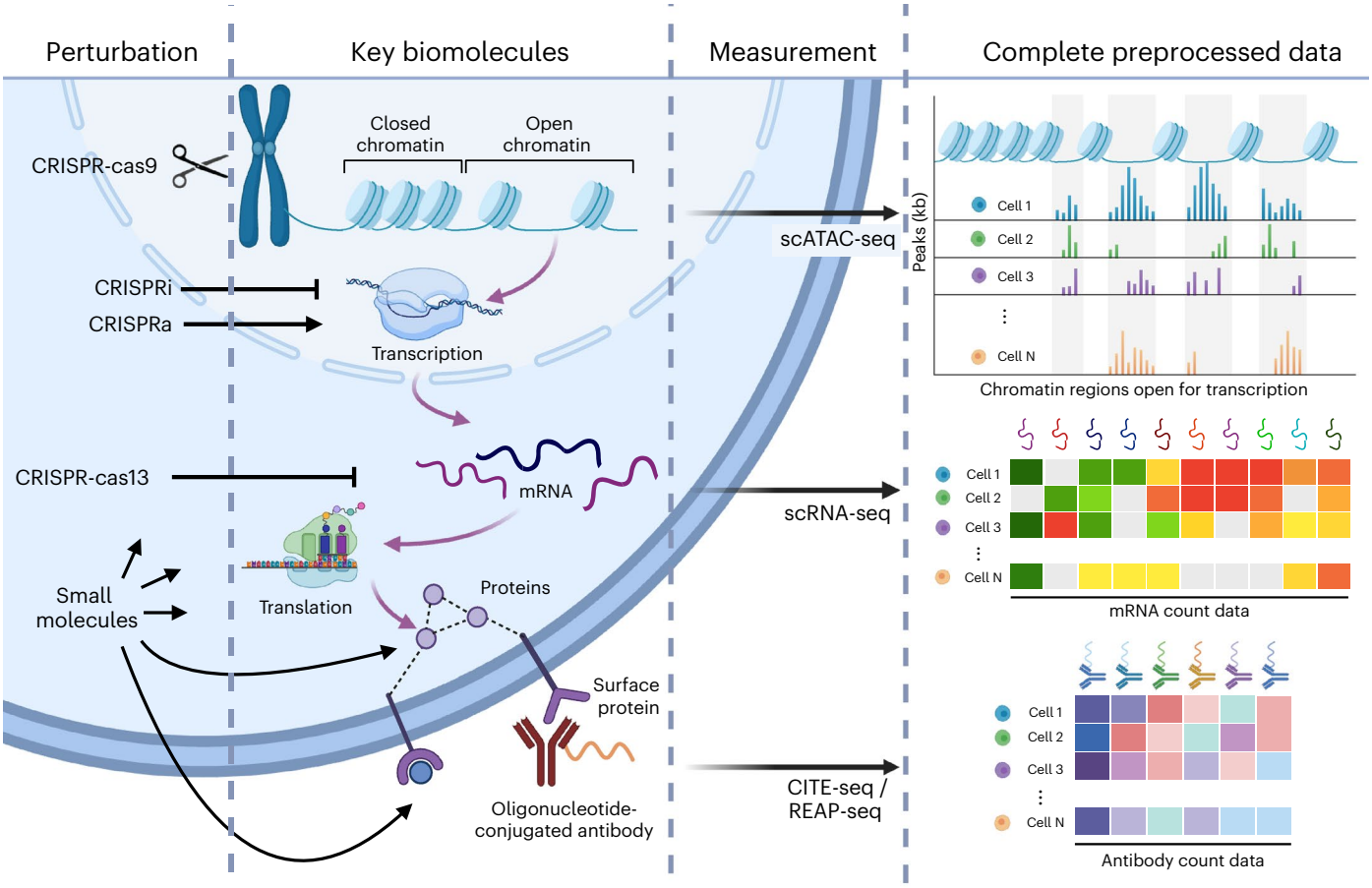

Fig. 1 | Perturbation–response profiling for single cells. Different perturbations act at different layers in the hierarchy of gene expression and protein production (purple arrows). Perturbations included in scPerturb include CRISPR-cas9, which directly perturbs the genome; CRISPRa, which activates transcription of a target gene; CRISPRi, which blocks transcription of targeted genes; CRISPR-cas13, which cleaves targeted mRNAs and promotes their degradation; cytokines that bind cell surface receptors; and small molecules that perturb various cellular mechanisms. Single-cell measurements probe the response to perturbation, also at different layers of gene expression: scATAC-seq directly probes chromatin state; scRNA-seq measures mRNA; and protein count data currently is typically obtained via antibodies bound to proteins. REAP-seq, RNA expression and protein sequencing.

transcripts, proteins, chromatin accessibility and, in some cases, phenotype[6]. Barcodes associated with unique CRISPR guide perturbations are read alongside single-cell RNA sequencing (scRNA-seq), CITE-seq (cellular indexing of transcriptomes and epitopes by sequencing) or scATAC-seq (single-cell sequencing assay for transposase-accessible chromatin) to identify each cell's perturbation condition[2,6–9].

Large-scale single-cell perturbation–response screens enable exploration of complex cellular behavior inaccessible in bulk measurements. Directionality in regulatory network models cannot be inferred without interventional or time-series data[10]. Experiments with targeted perturbations can be modeled as affecting individual nodes of a regulatory network model, enabling investigation of mechanistic processes and inference of regulatory interactions and their directionality[11]. Typically, however, perturbation datasets have been too small to elucidate the complexity of cellular systems; thus, accurately predictive models of regulatory interactions remain difficult to infer[12]. This limitation will be reduced as dataset size continues to increase. More directly, drug screens have been used to suggest therapeutic interventions by analyzing detailed molecular effects of targeted drugs, and designing new single or combinations of perturbations[13–15].

Reliable analysis of increasingly large perturbation datasets requires efficient statistical tools to harness large numbers of cells and perturbations. The inherently high dimensionality of perturbation–response data complicates calculation of distances between perturbations, as does cell-to-cell variation and data sparsity[16]. There is presently no convention for statistical comparison of response profiles in perturbation studies. Some studies carry out pseudo-bulk calculations by combining all cells in a given perturbation setting[1,7]. This means losing information about the cell-to-cell variation in response. Studies with mixtures of cell types have developed complex methods for quantifying similarity between heterogeneous cell populations[17–19]. Cell-based statistical measures can be used to identify successfully perturbed cells but do not currently quantify similarity of perturbation effects[2,9]. Ideally, statistical comparisons between perturbations and quantification of perturbation strength should be based on a multivariate distance measure between sets of cells. Such a distance measure describes the difference or similarity between the expression profiles of cells treated with distinct perturbations, thus inferring unique or shared mechanisms or identifying perturbation targets, which tend to produce similar shifts in molecular profiles[20,21]. Multiple distance measures for scRNA-seq have been explored by the single-cell community in recent years, including Wasserstein distance computed in an optimal transport framework[22,23], maximum mean discrepancy[24], neighborhood-based measures[17,18], and energy distance (E-distance)[20]. Here, we exclusively use E-distance, a fundamental statistical measure of distances between point clouds that can be used in a statistical test to identify strong or weak perturbations as well as to distinguish between perturbations affecting distinct cellular sub-processes. The associated energy test (E-test) is a statistically reliable tool for computational diagnostics of information content for a specific perturbation, and can

inform design of experiments and data selection for training statistical models of perturbation effects.

Large perturbation screens are specifically designed to study a particular system, such as a cell line, under a set of perturbations of interest. Over time, the field has accumulated a heterogeneous assortment of single-cell perturbation–response data with a wide range of different cell types, such as immortalized cell lines and induced pluripotent stem cell-derived models, and different perturbation technologies, including knockouts, activation, interference, base editing and prime editing[25]. Computational methods to efficiently harmonize these different perturbation datasets are needed. Such integrative analysis is complicated by batch effects and biological differences between primary tissue and cell culture[26,27]. Published computational methods for perturbation data are primarily focused on individual datasets[28–30]. Moving from single-dataset to multi-dataset analysis requires development of quantitative approaches to perturbation biology.

Although several large databases of perturbations with bulk readouts exist, single-cell perturbation technologies are newer and the data are not unified[31,32]. Existing collections of datasets are primarily a means for filtering and do not supply a unified format for perturbations[33–35]. However, unified datasets are key to developing generalizable machine learning methods and establishing multimodal data integration. A recent review and repository of single-cell perturbation data for machine learning lists 22 datasets but supplies cleaned and format-unified data for only six[36]. Unified frameworks for accessing single-cell data are in active development, but do not currently support perturbation datasets or standardize perturbation annotations[37,38].

We provide scPerturb, a resource of standardized datasets reporting targeted perturbations with single-cell readouts to facilitate the development and benchmarking of computational approaches in systems biology. We collected 44 publicly available perturbation–response datasets from 25 publications (Table 1 and Supplementary Fig. 1b). Our quantification of perturbation strength and comparison of experiment-specific variables, such as the number of perturbations and the number of cells per perturbation, may serve as a reference for optimal design of future single-cell experiments. We also describe E-distance and E-test as tools for statistical comparisons of sets of cells and benchmark their robustness and applicability for distinguishing perturbations across datasets and modalities. A web interface is accessible at scperturb.org, and packages for single-cell E-statistics are publicly available for both Python (PyPI: `scperturb`) and R (CRAN: `scperturbR`).

Results

Molecular readouts for the 44 single-cell perturbation–response datasets include transcript, protein and epigenetic profiles (Table 1 and Fig. 2a). Metadata were harmonized across datasets (Supplementary Table 2). Cells in 32 datasets underwent perturbation using CRISPR, and in 9 datasets the perturbation was done using drugs. While 32 datasets report scRNA-seq exclusively, we also include scATAC-seq from three publications, one with simultaneous protein measurements[39]. For each scRNA-seq dataset we supply count matrices, in which each cell has a perturbation annotation as well as quality control metrics. Three CITE-seq datasets have protein and RNA counts that are downloadable separately[6,9].

In contrast to scRNA-seq data, which can be represented naturally as counts per gene, there is no consensus representation of scATAC-seq data. In its raw form, scATAC-seq provides a noisy and very sparse description of chromatin accessibility over the entire genome. Following prior studies, we generated five feature sets of scATAC-seq data, each of which addresses different biological questions[40–42]. These features are intended to summarize chromatin accessibility over different types of biologically relevant genomic intervals (for example, gene neighborhood), or represent dense low-dimensional embeddings of the original data[43–45]. An investigation of how feature choice affects observed perturbation magnitude is included in Supplemental Note Section 7.

The measures of sample quality vary significantly across datasets (Fig. 2b). The total number of cells per dataset is usually restricted by experimental limitations although it has increased over time. Total unique molecular identifier (UMI) count per cell and number of genes per cell are calculated as described elsewhere[46]. These values are used for quality control in data analysis. The average sequencing depth, that is, the mean number of reads per cell, in each study affects the number of low-expression genes observed. Increasing sequencing depth increases the UMI counts measured even for low-expression genes, reducing the uncertainty associated with zero counts[34,47]. The overall number of recoverable UMI counts, usually estimated by sequencing saturation, also depends on the quality of the experiment: increasing sequencing depth alone cannot cover for loss of messenger RNA due to degradation. These differences can affect the distinguishability of perturbations and the performance of downstream analysis.

To compare and evaluate the effect and strength of perturbations in each dataset we used the E-distance, a statistical measure of the distance between two distributions, which provides intuition about the signal-to-noise ratio in a dataset[48]. For two groups of cells, it relates the distribution of distances of cells between the groups ('signal'), to the distribution of distances within each group ('noise'). More precisely, it compares the mean pairwise distance of cells between two different perturbations to the mean pairwise distance of cells within each of the two distributions (Fig. 3a; see Supplemental Note Section 4 for more detail). If the former is much larger than the latter, the two distributions are distinct. A low E-distance indicates that a perturbation did not induce a large shift in expression profiles, reflecting technical problems in the experiment, weak effect of the perturbation, or resistance to perturbation. Similar to related work[20], we compute the E-distance after principal component analysis (PCA) for dimensionality reduction[20]. Analysis of robustness with respect to details of data processing is provided in Supplemental Note Section 3.

The E-distance can also be used as a test statistic to assess whether cells after a perturbation are significantly different from unperturbed cells (Supplementary Table 3). The assessment is performed using the E-test, a Monte Carlo permutation test that uses the E-distance as a test statistic[48] (Methods). The exact value of the E-distance depends on dataset-specific parameters such as sequencing depth (Supplemental Note Section 4) and how exactly the cells are distributed; the E-test accounts for these differences by creating a null distribution using permutations of the data.

Interestingly, we found that E-distances between perturbed and unperturbed cells vary considerably across datasets (Fig. 3b). The dataset labeled 'NormanWeissman2019' had the largest mean E-distance between all perturbations[49] compared with datasets of similar size. In fact, expression profiles of most perturbations in this dataset were significantly different from those of unperturbed cells according to the E-test (Fig. 3c). Plausibly, this is in part caused by two-target perturbations using CRISPRa in that dataset: targeting the same gene with two single guides increases the chances of causing a considerable change in the transcript profile. Indeed, the three perturbations with highest E-distance are double perturbations while the three with the lowest E-distance are not. The corresponding UMAPs (uniform manifold approximation and projections) for these perturbations, computed using the same principal components used for the E-distance, provide a confirmatory visual intuition for high and low E-distances (Fig. 3e). Cells in the top three perturbations with the largest E-distance to unperturbed cells are easily distinguishable from the gray unperturbed cells, while cells from the bottom three weakest perturbations are part of a single, uniform cloud visually indistinguishable from the unperturbed cells. This illustrates that the smallest E-distance results from perturbations that have the least effect on the distribution of cells.

The E-distance can also be used to quantify similarity between different perturbations. For instance, there is a clear overlap of *CEBPA* and *KLF1* + *CEBPA* perturbed cells in the UMAP (Fig. 3e). This overlap

https://doi.org/10.1038/s41592-023-02144-y

Table 1 | Key metadata for datasets on scPerturb.org (more details in Supplementary Table 1)

Source paper	Modality	Perturbation type	No. of perturbations	No. of cells	UMI counts[a]	Genes[a]
Adamson[7]	RNA	CRISPRi	9; 20; 114	5,768; 15,006; 65,337	9,969; 25,082; 15,355	2,580; 4,304; 3,690
Aissa[68]	RNA	drugs	4	119,071	1,312	764
Chang[69]	RNA	drugs	4	42,277	18,961	5,278
Datlinger[1]	RNA	CRISPR-cas9 +TCR[b]	97	5,905	6,711	2,713
Datlinger[71]	RNA	CRISPR-cas9 +TCR[b]	48	39,194	1,282	364
Dixit[2]	RNA	CRISPR-cas9	31	51,898	13,974	3,080
Frangieh[6]	RNA+protein	CRISPR-cas9	249	218,331	10,988	3,314
Gasperini[54]	RNA	CRISPRi	43,314*; 39,087*; 16,531*	207,324; 47,650; 41,284	17,128	3,408; 3,795; 3,871
Gehring[19]	RNA	drugs	4	20,382	2,405	1,445
Liscovitch-Brauer[59]	ATAC	CRISPR-cas9	22; 84	8,723; 12,788		NA
McFarland[72]	RNA	drugs, CRISPR-cas9	18	182,875	17,976	3,780
Mimitou[73]	ATAC+protein	CRISPR-cas9	6	10,018		NA
Norman[49]	RNA	CRISPRa	237	111,445	13,855	3,233
Papalexi[9]	RNA+protein	CRISPR-cas9	11; 99	20,729; 8,984	11,815; 7,110	3,292; 2,530
Pierce[42]	ATAC	CRISPRi	41; 41; 41	22,488; 32,831; 18,025		NA
Replogle[20]	RNA	CRISPRi	2,058; 2,394; 9,867	310,385; 1,989,578; 247,914	13,207; 11,304; 11,940	3,618; 3,215; 3,441
Schiebinger[23]	RNA	cytokines	2; 3	68,339; 259,155	7,170; 10,271	2,358; 2,550
Schraivogel[74]	RNA	CRISPR-cas9	3,105*; 4,115*	120,310; 112,260	1,557; 1,218	60; 61
Shifrut[75]	RNA	CRISPR-cas9 +TCR[b]	49	52,236	5,382	1,894
Srivatsan[52]	RNA	drugs	5; 8; 189	24,262; 98,437; 799,317	4,207; 1,502; 1,538	2,280; 953; 925
Tian[76]	RNA	CRISPRi	27	182,790	13,878	4,266
Tian[21]	RNA	CRISPRa/i	101; 185	21,193; 32,300	10,263; 13,609	3,613; 4,521
Weinreb[77]	RNA	cytokines	5	65,075	3,229	1,333
Xie[78]	RNA	CRISPR-cas9	229	13,283	46,619	3,186
Zhao[79]	RNA	drugs	7	165,748	2,416	1,324

*Perturbation total treats perturbations A, B, and (A and B) as three unique perturbations. [a]Median per cell in datasets [b]T-cell receptor (TCR) stimulation.

is captured by a low E-distance: cells affected by these two perturbations are closer to each other than they are to unperturbed cells or to those from other perturbations (Fig. 3d and Supplementary Fig. 2a). We envision that the E-distance can be used as a suitable distance for other downstream tasks such as drug embeddings and clustering of perturbations, which could enable inference of functional similarity of perturbations by similarity in their induced molecular responses quantified by the E-distance.

As a detailed demonstration of the power of E-distance for analyzing perturbation datasets, we calculated pairwise E-distance between all pairs of perturbations in a dataset characterizing inhibitory immune checkpoints (Fig. 4). This study used CRISPR-cas9 to perturb genes encoding proteins involved in regulating programmed death-ligand (PD-L)1 (ref. 9). Hierarchical clustering of the resulting distance matrix produced two distinct groups of perturbations. The perturbations in the group more dissimilar to the unperturbed condition have a low E-distance to each other, suggesting a similar phenotype induced by perturbation of these genes (*IFNGR1*, *IFNGR2*, *JAK2*, *STAT1*). Indeed, the proteins encoded by these genes are all reported to be part of a signaling cascade upstream of interferon regulatory factor 1 (IRF1) and downstream of interferon-γ (IFNγ; ref. 50). In agreement with this, we observe that any disruption of a gene in this cascade leads to a similar outcome and, therefore, a similar transcriptome profile.

We investigate the robustness of E-distance and E-test scores to experimental and computational parameters using the scPerturb collection of annotation-harmonized single-cell perturbation datasets. We subsampled the number of cells per perturbation to create artificially smaller datasets, then examined how the E-distance and E-test results change. We introduce a bias correction to the E-distance that improves performance in low cell count regimes (Supplemental Note Section 1). We find that even after bias correction the E-distance increases as the number of cells per perturbation decreases, indicating that cells per perturbation should be standardized prior to calculating E-distances (Fig. 5a). This is due to the inability of PCA to adequately represent data in the low sample regime[51]. Despite the increase in E-distance with falling cell numbers, the number of significant perturbations correctly decreases with fewer cells, and only some datasets have saturated significance at the full number of cells in that dataset (Fig. 5b). This saturation point depends on perturbation strength and on dataset heterogeneity: if all cells are similar, a small set of cells will sufficiently describe every possible response to a perturbation. This suggests that, unsurprisingly, increasing sample size enables discovery of significant perturbations with smaller overall effects on transcripts.

Similarly, we subset the number of UMIs per cell, finding that E-distance increases as the UMI count per cell increases (Fig. 5c).

https://doi.org/10.1038/s41592-023-02144-y

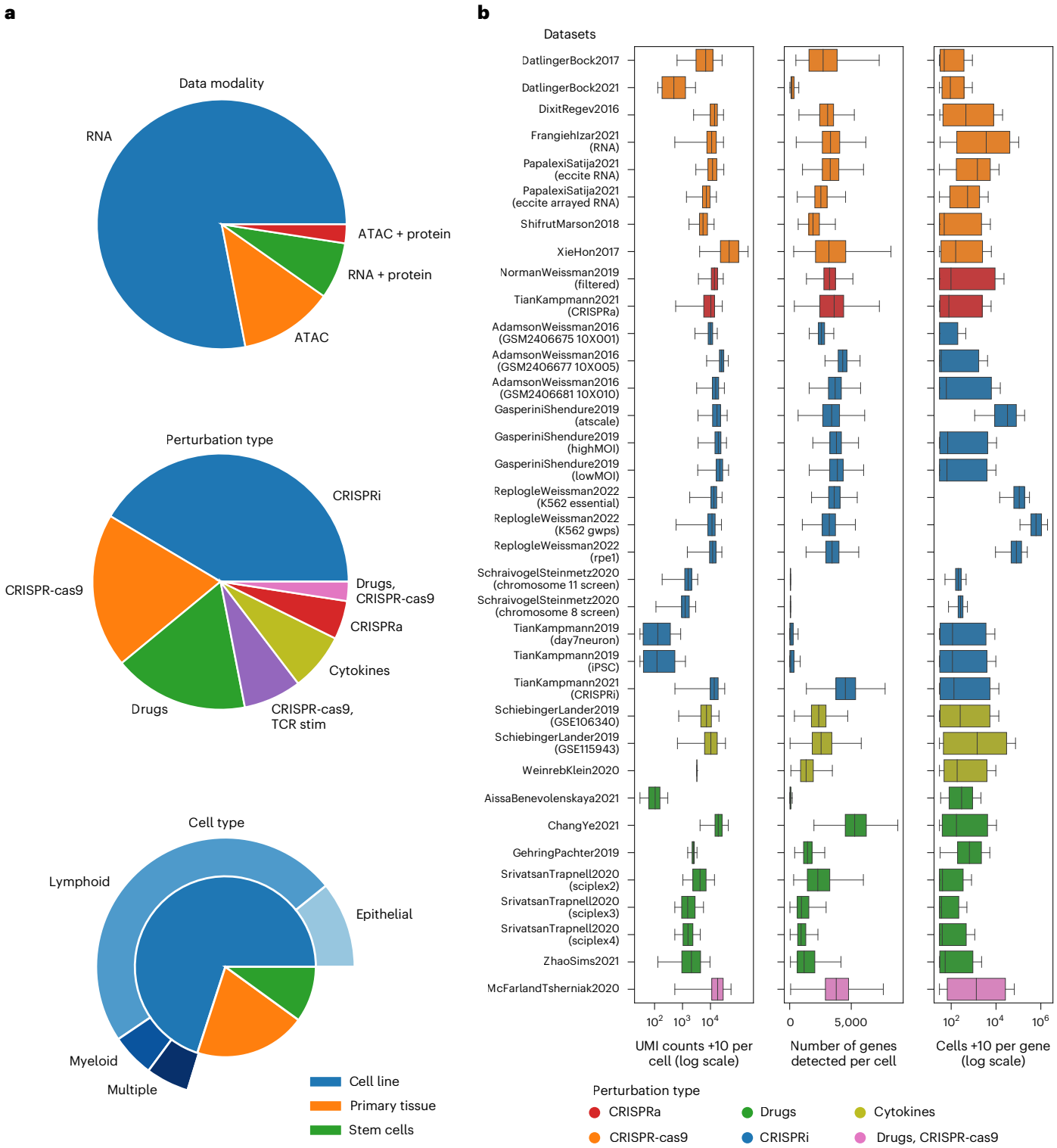

Fig. 2 | Single-cell perturbation–response datasets are diverse in type, size and quality. a, Datasets span a multitude of tissues and perturbation types. The majority of included datasets result from CRISPR (DNA cut, inhibition or activation) perturbations using cell lines derived from various cancers. The studies performed on cells from primary tissues generally use drug perturbations. Primary tissue refers to samples taken directly from patients or mice, sometimes with multiple cell types. **b**, Sequencing and cell count metrics across scPerturb perturbation datasets (rows), colored by perturbation type. From left to right: total RNA counts per cell (left); number of genes with at least one count in a cell (middle); number of cells with at least one count of a gene per gene (right). Most datasets have on average approximately 3,000 genes measured per cell, although some outlier datasets have significantly sparser coverage of genes. Number of cells per experiment (n) is listed in Table 1; average is 160,000; median, 65,000. Center line, median; box limits, upper and lower quartiles; whiskers, 1.5-fold the interquartile range. iPSC, induced pluripotent stem cell; MOI, multiplicity of infection.

https://doi.org/10.1038/s41592-023-02144-y

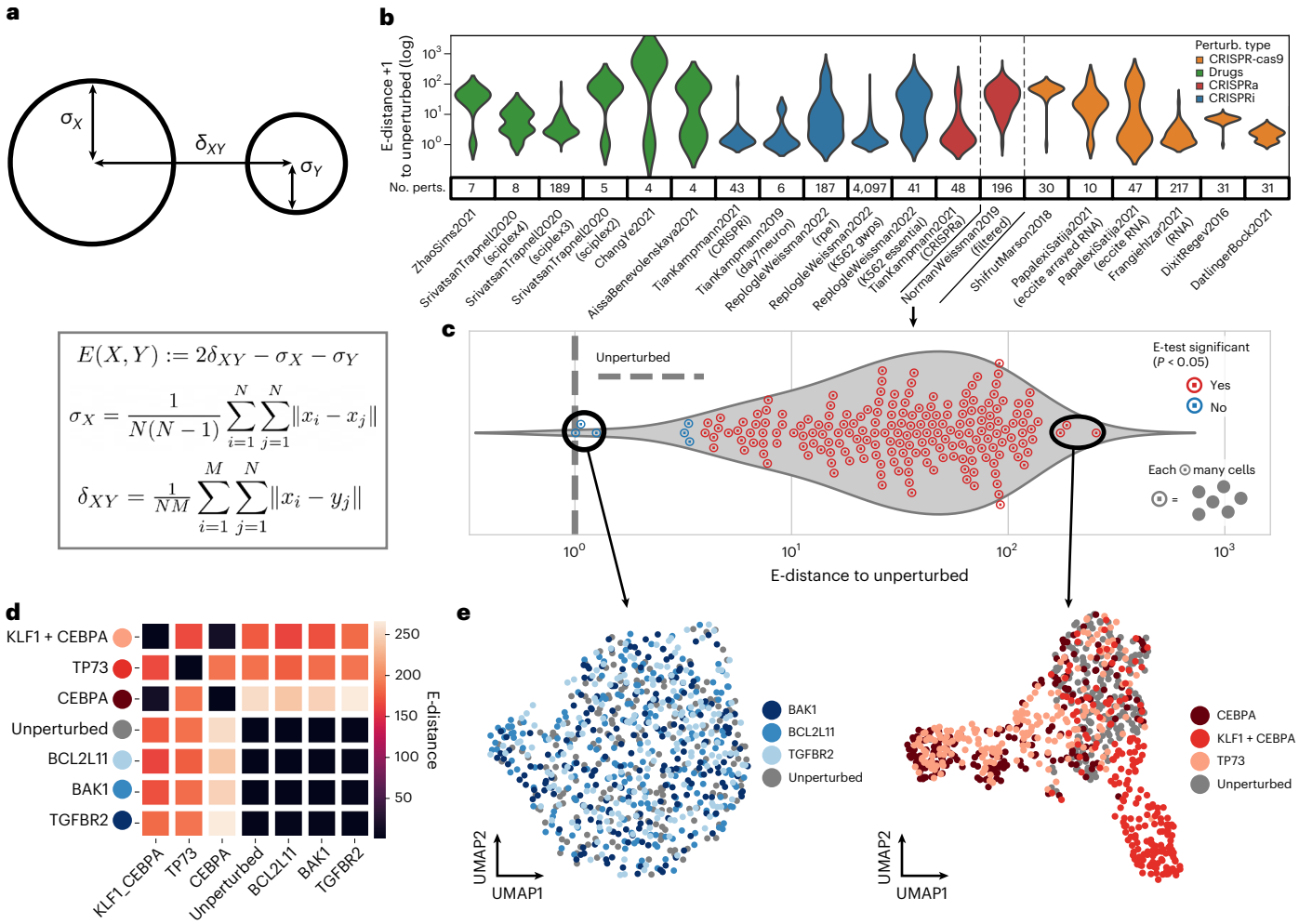

Fig. 3 | E-statistics describe distinctiveness of perturbations in single-cell data. a, Definition of E-distance, relating the width of cell distributions of high-dimensional molecular profiles to their distance from each other (see Methods). A large E-distance of perturbed cells from unperturbed indicates a strong change in molecular profile induced by the perturbation. **b**, Distribution of E-distances (for log scale, same in **c**) between perturbed and unperturbed cells across datasets. No. perts, number of perturbations per dataset. Note that this plot is best used to compare the shape of the E-distance distribution rather than the magnitude; the mean E-distance will vary significantly with other dataset properties. **c**–**e**, Analysis based on E-statistics for one selected dataset[49]. **c**, Distribution of E-distances between perturbed and unperturbed cells as in **b**. Each circled point is a perturbation, that is, it represents a set of cell profiles. Each perturbation was tested for significant E-distance to unperturbed (E-test). Distances and *P* values for each perturbation are listed in Supplementary Table 3. **d**, Pairwise E-distance matrix across the top and bottom three perturbations in **c** and the unperturbed cells. **e**, UMAP of single cells of the weakest (left, bottom three) and strongest (right, top three) perturbations.

The number of significant perturbations under the E-test, however, saturates at around 500 UMIs per cell, with most perturbations that were significant at the full measured read depth maintaining that significance even with far fewer counts per cell (Fig. 5d). The stability of E-test results with respect to UMI counts, in contrast to the actual E-distance value, demonstrates the necessity of the E-test, which uses a randomized control, as the appropriate statistical measure to evaluate the significance of perturbation effects. The optimal lower bounds on UMI and cell counts for a given experiment depend on downstream specific modeling tasks, as discussed in more detail elsewhere[12]. As a baseline for significant perturbations, as defined by the E-test, we suggest at least 200–500 cells per perturbation (Fig. 5b) and an average of 1,000 UMIs per cell (Fig. 5d) as an experimental guideline for distinguishable perturbations.

There are a few particularly notable datasets in the resource (Supplementary Fig. 2b). The most extensive drug dataset is sci-Plex 3, which includes 188 drugs tested across three cell lines[52]; 107 of those perturbations had significant effects on cell states according to E-test analysis (Supplementary Table 3). Five drugs in this dataset also appear in other drug perturbation datasets (Supplementary Table 4). We hope that future large-scale drug screens will enable more detailed analysis of drug response across different cell types and conditions. Another drug dataset applies combinations of three drug perturbations at varying concentrations across samples[19]. An example analysis of this dataset is in Supplemental Note Section 9. The most detailed CRISPR dataset is from a recently published study that carried out perturbation of 9,867 genes in human cells[20]. Containing >2.5 million cells, this dataset is the largest in our database, with the average number of cells, which each gene is detected in, being significantly higher than in other datasets. Notably, 138 CRISPR perturbations are seen in both RNA and ATAC datasets (Supplementary Table 5). More than 100 genes perturbed with CRISPRa in one dataset are perturbed with CRISPRi perturbations in another dataset of the same cell line, either in one publication[21] or across multiple studies[20,49]. The most frequently perturbed gene, *MYC*, is perturbed in nine datasets from three publications. Protein, RNA and ATAC readouts for CRISPRi perturbation of *MYC* are all available for K562 cells[6,20,42].

https://doi.org/10.1038/s41592-023-02144-y

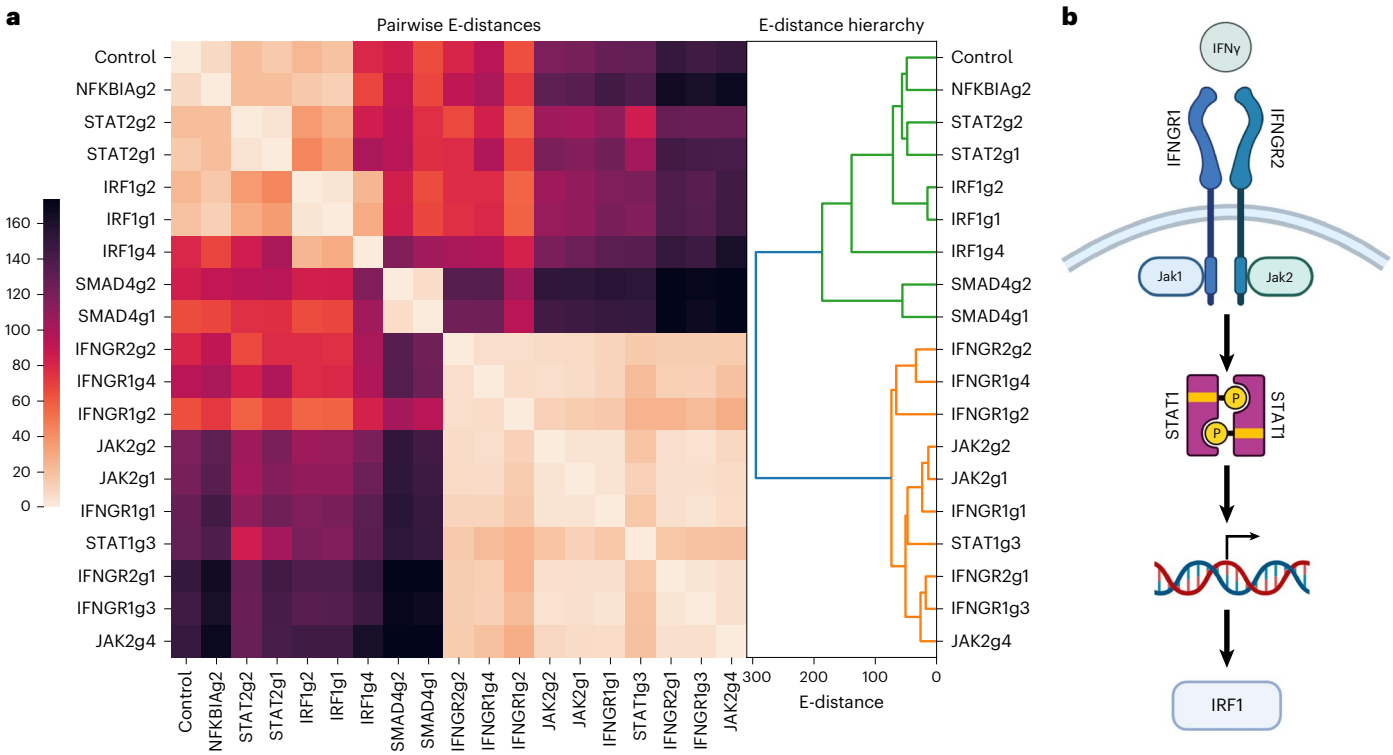

Fig. 4 | E-distance dissects perturbation hierarchy in data from Papalexi et al.[9]. a, E-distance between cells of all pairs of perturbations in the Papalexi et al. dataset[9]. Hierarchical clustering of this matrix produces two groups, one that is more similar to unperturbed cells (green) and one that has a stronger transcriptional change (orange). **b**, Signaling pathway downstream of the IFNγ receptor. Permutations of nodes upstream of IRF1 induce similar phenotypes.

Discussion

We present a dataset resource and an intuitive method for quantifying and analyzing single-cell perturbation datasets. Processed cellular response data with added quality control metrics are available on scPerturb.org. The uniform annotations in this resource enable data integration and benchmarking as well as exploration of the effects of shared perturbations across datasets. We introduce a bias-corrected E-distance for quantitatively comparing perturbations. We also investigate the effect of dataset-specific parameters on E-statistics, showing that E-statistics stabilize above 1,000 counts per cell and 200–500 cells per perturbation.

Although this work simplifies dataset access, joint analysis is limited by the complexity of data integration[27]. Across the eight drug datasets examined in this study, only five chemical agents occurred in more than one dataset (Supplementary Table 4). Shared gene targets are found more often across the CRISPR datasets (Supplementary Table 5). However, different experimental designs result in various covariates that may need to be accounted for in statistical testing. For example, high multiplicity-of-infection CRISPR screens with multiple targets per cell can complicate the calculation of distances[5,53,54]. In general, covariates arising from different experimental designs can affect the E-distance, and we recommend balancing cell numbers across experimental conditions if in doubt (Supplemental Note Section 8). Looking forward, this collection of datasets can be used to test data integration methods for perturbation biology, and it provides a unique opportunity to integrate datasets with overlapping perturbations and nominate machine learning benchmarks for data integration.

Lack of standardization in data sharing and processing across different research groups and studies hampered the creation of this resource. Although many processed datasets were available on the National Center for Biotechnology Information (NCBI) Gene Expression Omnibus (GEO)[55], there is no standard format for sharing CRISPR barcode assignments and other metadata. Starting the analysis from sequencing reads may have improved the interoperability of datasets in this resource, but guide assignment procedures and demultiplexing algorithms are experimental set-up specific. For scATAC, data comparison is hindered by the lack of a standard method for feature assignment (Methods and Supplemental Note Section 7). In particular, for scATAC feature assignments specific to CRISPR perturbations, known loci of action could be used to improve feature calls[40]. For all data types, many datasets supplied only processed data, or raw data were available only after institutional clearance. Adding more datasets to this resource, or the creation of similar resources in the future, would be easier if there were standard formats for sharing perturbation data, and, more generally, standard formats for sharing single-cell annotations. While this report can provide some guidance, a community-wide discussion on standardization of such data is urgently needed, as was done for proteomic data[56].

Such a standardization effort would enable simpler addition of datasets to the resource. Until universal standards are established, we encourage data creators to format their data following the guidelines in Supplementary Table 2 and contact the authors, for example, via the scPerturb website or associated GitHub repository, for inclusion. We anticipate that recent technological advances will decrease experimental costs and result in more new datasets, with additional experiment-specific analysis methods needed to convert from new highly multiplexed readouts into a standardized format[53]. The existing scPerturb database will be available archivally via Zenodo (see Data Availability), and we are committed to maintaining the resource with additional datasets for at least 3–4 years.

Beyond that timeline, it is difficult to predict what forms of data will be of primary interest to the community. At present, the resource consists predominantly of unimodal scRNA-seq data (Fig. 2a). The relatively smaller inclusion of scATAC-seq and other data types limits the resource's utility for researchers working in epigenomics and gene

https://doi.org/10.1038/s41592-023-02144-y

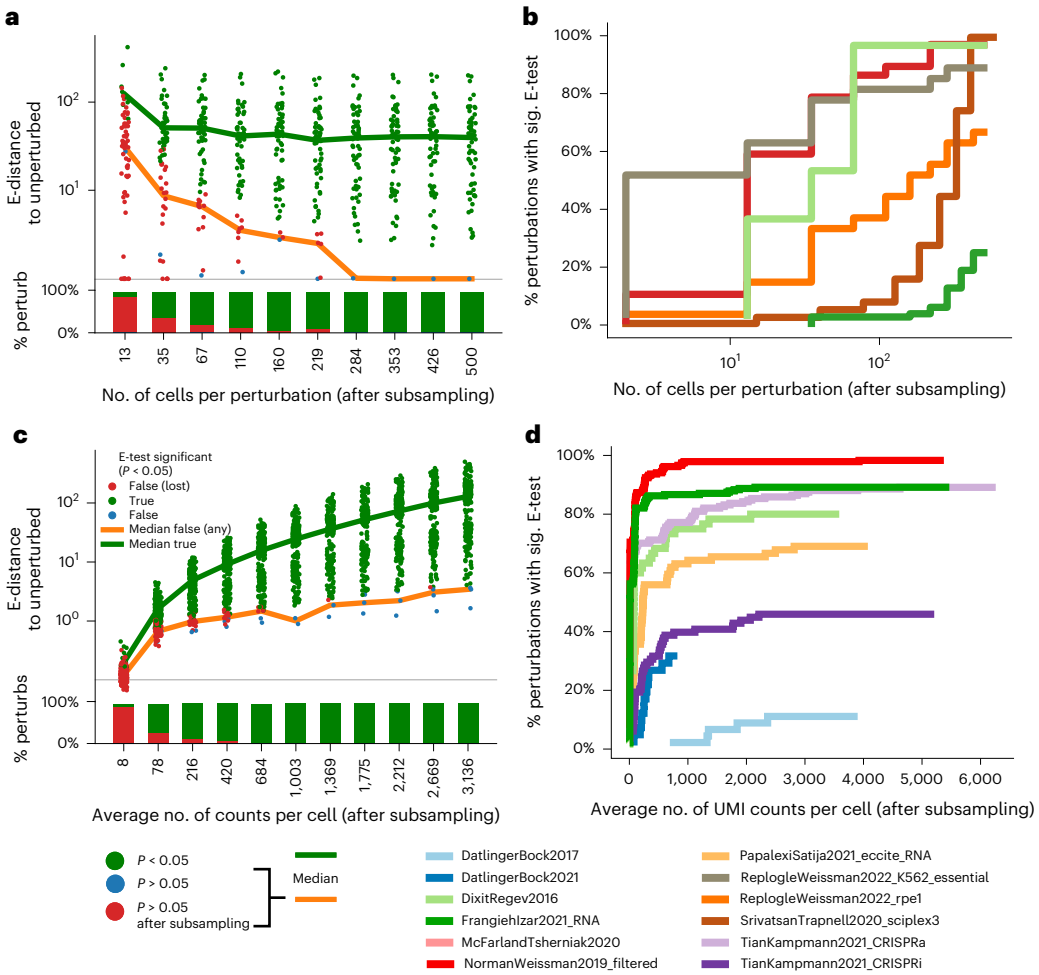

Fig. 5 | Effect of subsampling UMI counts per cell and number of cells per perturbation on E-statistics. a, E-distance of each perturbation to unperturbed in the Norman et al. dataset[49] while subsampling the number of cells per perturbation. Color indicates E-test results; 'significance lost': perturbation significant when all cells are considered, but not significant after subsampling. The E-test loses significance with lower cell numbers while the E-distance actually increases. **b**, The overall number of perturbations with significant (sig.) E-test decreases when subsampling cells per perturbation. **c**, As in **a** but subsampling UMI counts per cell while keeping the number of cells constant. E-test significance was lost and E-distance to unperturbed dropped as the overall signal deteriorated with removal of UMI counts. **d**, As in **b** but subsampling UMI counts per cell while keeping the number of cells constant.

regulation. Moreover, there is increasing interest in spatial techniques, including single-cell resolution spatial transcriptomics, epigenomics and proteomics[57]. The sharing of spatial data is hampered by large file sizes and non-standardized analysis pipelines[58]. A broader effort such as scPerturb might be needed in the future to specifically address the complexity of annotation-harmonizing spatial datasets.

Experiment design choices, such as the optimal number of cells per perturbation and the sequencing depth for each cell, depend on the questions that a particular perturbation study is intended to answer, and on the strength and uniqueness of the gene expression changes caused by the perturbations. Unfortunately, it is difficult to ascertain to what extent low E-distances between perturbed and unperturbed cells are caused by technical noise or simply weak perturbation effects compared with biological variation in groups of cells before and after perturbation. Increasing the dose or varying the time between perturbation start and collection of the cells may be advisable to increase the signal-to-noise ratio without sequencing more cells. For perturbation distinguishability as defined by the E-test, regardless of experiment parameters, we recommend measuring at least 200–500 cells per perturbation and an average of 1,000 UMIs per cell.

We envision that the scPerturb collection of datasets and the suggested E-statistics analytic framework will be valuable starting points for analysis of single-cell perturbation data. The unified annotations and perturbation significance testing should prove especially useful to the machine learning community for training computational models on this data. We expect that additional datasets and experimental perturbation methods in the future will enable the community to develop computational approaches to exploit the richness of single-cell perturbation data, aiming at the development of increasingly accurate and quantitatively predictive models of cell biological processes and the design of targeted interventions for investigational or therapeutic purposes.

Online content

Any methods, additional references, Nature Portfolio reporting summaries, source data, extended data, supplementary information, acknowledgements, peer review information; details of author contributions and competing interests; and statements of data and code availability are available at https://doi.org/10.1038/s41592-023-02144-y.

References

1. Datlinger, P. et al. Pooled CRISPR screening with single-cell transcriptome readout. *Nat. Methods* **14**, 297–301 (2017).

2. Dixit, A., Parnas, O., Li, B. & Chen, J. Perturb-seq: dissecting molecular circuits with scalable single-cell RNA profiling of pooled genetic screens. *Cell* **167**, 1853–1866 (2016).
3. Jaitin, D. A. et al. Dissecting immune circuits by linking CRISPR-pooled screens with single-cell RNA-seq. *Cell* **167**, 1883–1896 (2016).
4. Gilbert, L. A. et al. Genome-scale CRISPR-mediated control of gene repression and activation. *Cell* **159**, 647–661 (2014).
5. Wessels, H.-H. et al. Efficient combinatorial targeting of RNA transcripts in single cells with Cas13 RNA Perturb-seq. *Nat. Methods* **20**, 86–94 (2023).
6. Frangieh, C. J. et al. Multimodal pooled Perturb-CITE-seq screens in patient models define mechanisms of cancer immune evasion. *Nat. Genet.* **53**, 332–341 (2021).
7. Adamson, B. et al. A multiplexed single-cell CRISPR screening platform enables systematic dissection of the unfolded protein response. *Cell* **167**, 1867–1882 (2016).
8. Rubin, A. J. et al. Coupled single-cell CRISPR screening and epigenomic profiling reveals causal gene regulatory networks. *Cell* **176**, 361–376 (2019).
9. Papalexi, E. et al. Characterizing the molecular regulation of inhibitory immune checkpoints with multimodal single-cell screens. *Nat. Genet.* **53**, 322–331 (2021).
10. Gross, T., Wongchenko, M. J., Yan, Y. & Blüthgen, N. Robust network inference using response logic. *Bioinformatics* **35**, i634–i642 (2019).
11. Pratapa, A., Jalihal, A. P., Law, J. N., Bharadwaj, A. & Murali, T. M. Benchmarking algorithms for gene regulatory network inference from single-cell transcriptomic data. *Nat. Methods* **17**, 147–154 (2020).
12. Gross, T. & Blüthgen, N. Identifiability and experimental design in perturbation studies. *Bioinformatics* **36**, i482–i489 (2020).
13. Bertin, P. et al. RECOVER: sequential model optimization platform for combination drug repurposing identifies novel synergistic compounds in vitro. Preprint at https://doi.org/10.48550/arXiv.2202.04202 (2022).
14. Franz, A. et al. Molecular response to PARP1 inhibition in ovarian cancer cells as determined by mass spectrometry based proteomics. *J. Ovarian Res.* **14**, 140 (2021).
15. Preuer, K. et al. DeepSynergy: predicting anti-cancer drug synergy with deep learning. *Bioinformatics* **34**, 1538–1546 (2018).
16. Kharchenko, P. V. The triumphs and limitations of computational methods for scRNA-seq. *Nat. Methods* **18**, 723–732 (2021).
17. Burkhardt, D. B. et al. Quantifying the effect of experimental perturbations at single-cell resolution. *Nat. Biotechnol.* **39**, 619–629 (2021).
18. Dann, E., Henderson, N. C., Teichmann, S. A., Morgan, M. D. & Marioni, J. C. Differential abundance testing on single-cell data using k-nearest neighbor graphs. *Nat. Biotechnol.* **40**, 245–253 (2022).
19. Gehring, J., Park, J. H., Chen, S., Thomson, M. & Pachter, L. Highly multiplexed single-cell RNA-seq by DNA oligonucleotide tagging of cellular proteins. *Nat. Biotechnol.* **38**, 35–38 (2020).
20. Replogle, J. M. et al. Mapping information-rich genotype–phenotype landscapes with genome-scale Perturb-seq. *Cell* **185**, 2559–2575 (2022).
21. Tian, R. et al. Genome-wide CRISPRi/a screens in human neurons link lysosomal failure to ferroptosis. *Nat. Neurosci.* **24**, 1020–1034 (2021).
22. Chen, W. S. et al. Uncovering axes of variation among single-cell cancer specimens. *Nat. Methods* **17**, 302–310 (2020).
23. Schiebinger, G. et al. Optimal-transport analysis of single-cell gene expression identifies developmental trajectories in reprogramming. *Cell* **176**, 928–943 (2019).
24. Lotfollahi, M., Naghipourfar, M., Theis, F. J. & Wolf, F. A. Conditional out-of-distribution generation for unpaired data using transfer VAE. *Bioinformatics* **36**, i610–i617 (2020).
25. Przybyla, L. & Gilbert, L. A. A new era in functional genomics screens. *Nat. Rev. Genet.* **23**, 89–103 (2022).
26. Forcato, M., Romano, O. & Bicciato, S. Computational methods for the integrative analysis of single-cell data. *Brief. Bioinform.* **22**, 20–29 (2021).
27. Luecken, M. D. et al. Benchmarking atlas-level data integration in single-cell genomics. *Nat. Methods* **19**, 41–50 (2022).
28. Duan, B. et al. Model-based understanding of single-cell CRISPR screening. *Nat. Commun.* **10**, 2233 (2019).
29. Jin, K. et al. CellDrift: inferring perturbation responses in temporally-sampled single cell data. *Brief. Bioinform.* **23**, bbac324 (2022).
30. Lotfollahi, M., Wolf, F. A. & Theis, F. J. scGen predicts single-cell perturbation responses. *Nat. Methods* **16**, 715–721 (2019).
31. Stathias, V. et al. LINCS Data Portal 2.0: next generation access point for perturbation–response signatures. *Nucleic Acids Res.* **48**, D431–D439 (2020).
32. Tsherniak, A. et al. Defining a cancer dependency map. *Cell* **170**, 564–576 (2017).
33. Lance, C. et al. Multimodal single cell data integration challenge: results and lessons learned. Preprint at https://doi.org/10.1101/2022.04.11.487796 (2022).
34. Svensson, V., da Veiga Beltrame, E. & Pachter, L. A curated database reveals trends in single-cell transcriptomics. *Database* **2020**, baaa073 (2020).
35. Broad Institute. Single Cell Portal. https://singlecell.broadinstitute.org/single_cell (2022).
36. Ji, Y., Lotfollahi, M., Wolf, F. A. & Theis, F. J. Machine learning for perturbational single-cell omics. *Cell Syst.* **12**, 522–537 (2021).
37. Fischer, D. S. et al. Sfaira accelerates data and model reuse in single cell genomics. *Genome Biol.* **22**, 248 (2021).
38. Chan Zuckerberg CELLxGENE Discover. Cellxgene Data Portal. https://cellxgene.cziscience.com/
39. Mimitou, E. P. et al. Multiplexed detection of proteins, transcriptomes, clonotypes and CRISPR perturbations in single cells. *Nat. Methods* **16**, 409–412 (2019).
40. Chen, H. et al. Assessment of computational methods for the analysis of single-cell ATAC-seq data. *Genome Biol.* **20**, 241 (2019).
41. Granja, J. M. et al. ArchR is a scalable software package for integrative single-cell chromatin accessibility analysis. *Nat. Genet.* **53**, 403–411 (2021).
42. Pierce, S. E., Granja, J. M. & Greenleaf, W. J. High-throughput single-cell chromatin accessibility CRISPR screens enable unbiased identification of regulatory networks in cancer. *Nat. Commun.* **12**, 2969 (2021).
43. Buenrostro, J. D. et al. Single-cell chromatin accessibility reveals principles of regulatory variation. *Nature* **523**, 486–490 (2015).
44. Cusanovich, D. A. et al. Multiplex single-cell profiling of chromatin accessibility by combinatorial cellular indexing. *Science* **348**, 910–914 (2015).
45. Schep, A. N., Wu, B., Buenrostro, J. D. & Greenleaf, W. J. chromVAR: inferring transcription-factor-associated accessibility from single-cell epigenomic data. *Nat. Methods* **14**, 975–978 (2017).
46. Luecken, M. D. & Theis, F. J. Current best practices in single-cell RNA-seq analysis: a tutorial. *Mol. Syst. Biol.* **15**, e8746 (2019).
47. Haque, A., Engel, J., Teichmann, S. A. & Lönnberg, T. A practical guide to single-cell RNA-sequencing for biomedical research and clinical applications. *Genome Med.* **9**, 75 (2017).
48. Székely, G. J. & Rizzo, M. L. Energy statistics: a class of statistics based on distances. *J. Stat. Plan. Inference* **143**, 1249–1272 (2013).

49. Norman, T. M. et al. Exploring genetic interaction manifolds constructed from rich single-cell phenotypes. *Science* **365**, 786–793 (2019).
50. Schroder, K., Hertzog, P. J., Ravasi, T. & Hume, D. A. Interferon-γ: an overview of signals, mechanisms and functions. *J. Leukoc. Biol.* **75**, 163–189 (2004).
51. Jung, S. & Marron, J. S. PCA consistency in high dimension, low sample size context. *Ann. Stat.* **37**, 4104–4130 (2009).
52. Srivatsan, S. R. et al. Massively multiplex chemical transcriptomics at single-cell resolution. *Science* **367**, 45–51 (2020).
53. Yao, D. et al. Scalable genetic screening for regulatory circuits using compressed Perturb-seq. *Nat. Biotechnol.* https://doi.org/10.1038/s41587-023-01964-9 (2023).
54. Gasperini, M. et al. A genome-wide framework for mapping gene regulation via cellular genetic screens. *Cell* **176**, 377–390 (2019).
55. Barrett, T. et al. NCBI GEO: archive for functional genomics data sets – update. *Nucleic Acids Res.* **41**, D991–D995 (2013).
56. Gatto, L. et al. Initial recommendations for performing, benchmarking and reporting single-cell proteomics experiments. *Nat. Methods* **20**, 375–386 (2023).
57. Tian, L., Chen, F. & Macosko, E. Z. The expanding vistas of spatial transcriptomics. *Nat. Biotechnol.* **41**, 773–782 (2023).
58. Bredikhin, D., Kats, I. & Stegle, O. MUON: multimodal omics analysis framework. *Genome Biol.* **23**, 42 (2022).
59. Liscovitch-Brauer, N. et al. Profiling the genetic determinants of chromatin accessibility with scalable single-cell CRISPR screens. *Nat. Biotechnol.* **39**, 1270–1277 (2021).
68. Aissa, A. F. et al. Single-cell transcriptional changes associated with drug tolerance and response to combination therapies in cancer. *Nat. Commun.* **12**, 1628 (2021).
69. Chang, M. T. et al. Identifying transcriptional programs underlying cancer drug response with TraCe-seq. *Nat. Biotechnol.* **40**, 86–93 (2022).
71. Datlinger, P. et al. Ultra-high-throughput single-cell RNA sequencing and perturbation screening with combinatorial fluidic indexing. *Nat. Methods* **18**, 635–642 (2021).
72. McFarland, J. M. et al. Multiplexed single-cell transcriptional response profiling to define cancer vulnerabilities and therapeutic mechanism of action. *Nat. Commun.* **11**, 4296 (2020).
73. Mimitou, E. P. et al. Scalable, multimodal profiling of chromatin accessibility, gene expression and protein levels in single cells. *Nat. Biotechnol.* **39**, 1246–1258 (2021).
74. Schraivogel, D. et al. Targeted Perturb-seq enables genome-scale genetic screens in single cells. *Nat. Methods* **17**, 629–635 (2020).
75. Shifrut, E. et al. Genome-wide CRISPR screens in primary human T cells reveal key regulators of immune function. *Cell* **175**, 1958–1971 (2018).
76. Tian, R. et al. CRISPR interference-based platform for multimodal genetic screens in human iPSC-derived neurons. *Neuron* **104**, 239–255 (2019).
77. Weinreb, C., Rodriguez-Fraticelli, A., Camargo, F. D. & Klein, A. M. Lineage tracing on transcriptional landscapes links state to fate during differentiation. *Science* **367**, eaaw3381 (2020).
78. Xie, S., Duan, J., Li, B., Zhou, P. & Hon, G. C. Multiplexed engineering and analysis of combinatorial enhancer activity in single cells. *Mol. Cell* **66**, 285–299 (2017).
79. Zhao, W. et al. Deconvolution of cell type-specific drug responses in human tumor tissue with single-cell RNA-seq. *Genome Med.* **13**, 82 (2021).

Methods

scATAC-seq

Data acquisition. We included scATAC-seq data from three different sources: Spear-ATAC[42], CRISPR-sciATAC[59] and ASAP-seq[39]. All data that were used in our analysis can be programmatically downloaded with scripts that are provided in our code repository (https://github.com/sanderlab/scPerturb).

scATAC-seq is a biomolecular technique to assess chromatin accessibility in single cells[43,44]. The starting point of our data processing pipeline is BED-like tabular fragment files, in which each line represents a unique ATAC-seq fragment captured by the assay. Each fragment is mapped to a genomic interval and a cell barcode. The goal of our pipeline is to extract standardized features from this information. Those are: embeddings derived from latent-semantic-indexing (LSI)[44] with 30 dimensions for each cell (a dimensionality reduction method that is well-suited to the sparsity of the data); gene scores that measure the chromatin accessibility around each gene for each cell (the weighted sum of fragment counts around the neighborhood of a gene's transcription start site, where more distant counts contribute less); a peak–barcode matrix that quantifies the chromatin accessibility at (dataset-specific) consensus peaks (genomic intervals) for each cell; chromVAR scores[45], which quantify the activity of a set of transcription factors for each cell, using transcription factor footprints as defined in ref. 60; and marker-peaks per perturbation target, which quantifies the differential regulation of highly variable peaks for each type of perturbation.

These features were computed using the ArchR framework v1.0.1 (ref. 41) with standard parameters unless otherwise stated. We provide each feature set as a dedicated h5ad file on scperturb.org, and our analysis mostly follows the pipeline proposed in Spear-ATAC[42], as detailed below.

Note that these features were originally developed for scATAC-seq data on non-perturbed cells, with goals such as the identification of cell type, discovery of cell type-specific regulatory elements, or reconstruction of cellular differentiation trajectories[43,61].

Pre-processing. Filtering of low-quality cells. To ensure a consistent and homogenous quality throughout the different datasets, we filtered out cells with fewer than 1,000 and more than 100,000 mapped fragments. Furthermore, we required a minimum transcription start site enrichment score of 4 to ensure a sufficient signal-to-noise ratio. See the createArrowFile function in ArchR for details.

For the Spear-ATAC dataset we ran ArchR's getValidBarcodes function on processed 10x Cell Ranger files to subset the dataset to valid barcodes. For the other datasets these files were unavailable, and we relied on the original authors' pre-processing of barcodes.

Assignment of single-guide RNAs to barcodes. For the Spear-ATAC[42] and CRISPR_sciATAC[59] datasets we had access to cell barcode–sgRNA count matrices (see original publications for details). We assigned the sgRNA with the highest counts to a cell barcode if the sgRNA count exceeded 20 and if that sgRNA comprised at least 80% of all sgRNA counts. Cells that could not be assigned an sgRNA were left in the dataset. For the ASAP-seq dataset a barcode–sgRNA matrix was not available. Instead, we relied on an sgRNA assignment downloaded from the study's GitHub repository[32].

Feature computation. All features described in the overview above were computed with ArchR functions. For details see the fragments2outputs.R script in our code repository, in the Data Availability section.

scRNA-seq

Data acquisition. Datasets were downloaded from public databases following data availability directions in the source papers. When available from the authors, unnormalized preprocessed cell-by-gene matrices were used. Supplemental information from the papers were used in data analysis when applicable.

Data processing. Analysis was initiated using unfiltered, unnormalized cell-by-gene matrices as provided by source papers. For one dataset, preprocessed cell-by-gene matrices were unavailable; pre-processing was performed following the procedure outlined in the original paper, directly using supplied code[19]. For datasets with cell barcodes, barcode assignments for cells were taken from the original paper when available; when not available, barcode assignment was performed as described in the methods section of the relevant paper. If multiple guides were assigned to the same cell, the guides were listed in decreasing order of counts in the final data object. The code used to process each individual dataset, including barcode assignment, is available in our code repository.

Datasets were imported into AnnData objects using Scanpy (v1.7.2–1.9.1)[62]. Metadata were taken from the original papers when available. For cell lines, information on sex, age, disease and origin were taken from Cellosaurus[63]. Metadata columns are described in Supplementary Table 2. Items listed in bold are included for all datasets.

Datasets are stored as .h5ad files. Code is supplied in our code repository for the import of .mtx files into Seurat.

Data analysis. Before calculating the E-distances (Fig. 4), cells and genes were filtered using Scanpy (v1.7.2–1.9.1)[62]. All .h5ad objects published on the resource were saved using Scanpy v1.9.1. Cells were retained if they had a minimum of 1,000 UMIs, and genes, with a minimum of 50 cells. A total of 2,000 highly variable genes were selected using `scanpy.pp.find_variable_genes` with flavor seurat_v3. We normalized the count matrix using `scanpy.pp.normalize_total` and log-transformed the data using `scanpy.pp.log1p`; we did not z-scale the data. Next, we computed PCA based on the highly variable genes. The E-distances were computed in that PCA space using 50 components and Euclidean distance. To avoid problems due to different numbers of cells per perturbation, we subsampled each dataset such that all perturbations had the same number of cells. We removed all perturbations with fewer than 50 cells and then subsampled to the number of cells in the smallest perturbation left after filtering. Large parts of our analysis were parallelized as workflows using Snakemake[64]. For applications of E-distance to datasets with confounding factors such as batch effect, we recommend correcting for these factors prior to PCA.

E-distance. The E-distance is a statistical distance between high-dimensional distributions and has been used to define a multivariate two-sample test, called the energy test (E-test)[65]. It is more commonly known as energy distance, stemming from the original interpretation using gravitational energy in physics. Formally, it contextualizes the notion that two distributions of points in a high-dimensional space are distinguishable if they are far apart compared with the width of both distributions (Fig. 3a). More specifically,

Let $x_1, \ldots, x_N \in \mathbb{R}^d$ and $y_1, \ldots, y_M \in \mathbb{R}^d$ be samples from two distributions X, Y, corresponding to two sets of N and M cells, respectively.

We define

$$\delta_{XY} = \frac{1}{NM} \sum_{i=1}^{N} \sum_{j=1}^{M} ||x_i - y_j||$$

$$\sigma_X = \frac{1}{N^2} \sum_{i=1}^{N} \sum_{j=1}^{N} ||x_i - x_j||$$

and σ_Y defined accordingly. We used the squared Euclidean distance when calculating cell-wise distances. Intuitively, δ_{XY} is the mean distance between cells from the two distributions, while σ_X describes the

mean distance between a cell from X to another cell from X. The energy distance between X and Y is defined as:

$$E(X,Y) := 2\delta_{XY} - \sigma_X - \sigma_Y$$

For the bias-corrected energy distance, described in detail in the Supplemental Note, we define

$$\sigma_X = \frac{1}{N(N-1)} \sum_{i=1}^{N} \sum_{j=1}^{N} ||x_i - x_j||$$

With the exception of the calculations for Fig. 5c and Fig. 5d, which use the standard E-distance, all calculations use the bias-corrected form of the E-distance.

E-test calculation. The E-test was performed as a Monte Carlo permutation test using E-distance as the test statistic. For each dataset and each perturbation in that dataset, we took the cells and combined them with the unperturbed cells. Then, we shuffled the perturbation labels and computed the E-distance between the two resulting groups. We repeated this process 10,000 times. The number of times that this shuffled E-distance to the unperturbed group was larger than the unshuffled E-distance, divided by 10,000, yields a P value corresponding to a one-sided test of difference, which we report for almost all datasets in our resource (Supplementary Table 3). We corrected for multiple testing using the Holm–Sidak method per dataset.

Subsampling analysis. At each subsampling point we computed detailed E-statistics (E-distances, delta, sigma, E-test results) for the E-distance from each perturbation to the corresponding unperturbed cells of that dataset using PCA with 50 components based on 2,000 highly variable genes, except when specified otherwise. We downsampled raw UMI counts using the function `scanpy.pp.downsample_counts` on raw counts, then preprocessed (normalized, log1p-transformed, and so on) the data as previously described. Cells were downsampled to the same number at each subsampling step across all perturbations to avoid comparability issues. If possible, we recalculated the PCA while keeping the highly variable genes originally obtained from the complete dataset. Figure 5c,d was computed as a running loss of E-test significance ($P < 0.05$) of formerly (that is, prior to any subsampling) significant perturbations while subsampling, then normalized across datasets through division by the total number of formally significant perturbations in that dataset.

Advice for single-cell perturbation analysis. Resource users should be aware that memory requirements quickly become a limiting factor, especially with the newer, larger datasets, such as ReplogleWeissman2022 with >2.5 million cells across more than 9,000 perturbations[20]. For example, the E-distance presented here for calculating distances between perturbed sets of cells relies on PCA, but computing PCA for all data in this dataset was not possible with 500 GB of memory without modifications to accelerate computation. In future, computational methods will need to be modified as in ref. 66 to reduce memory load, or datasets will need to be subsampled. Additionally, the .h5ad datasets shared in this resource can be programmatically accessed using .h5py, and perturbations of interest extracted without requiring full dataset access.

To our knowledge, best practices have not yet been established for analysis of single-cell perturbation data. DESeq2 is frequently used for differential expression testing, given that it can be applied to pseudo-bulk profiles of each perturbation[67]. An optional next step would be enrichment analysis of the resulting genes. Averaging single-cell measurements over cells per perturbation simplifies analysis and reduces the effect of measurement noise significantly but comes at the cost of removing all system-intrinsic biologically relevant information in cell-to-cell variation. In many studies, these average profiles are then embedded using a dimensionality reduction method of choice and subsequently clustered to identify groups of perturbations with potentially similar targets[20,49].

Reporting summary

Further information on research design is available in the Nature Portfolio Reporting Summary linked to this article.

Data availability

The website scperturb.org stores harmonized datasets with the following: scRNA-seq and antibody-based protein datasets: .h5ad files; scATAC-seq: multiple different feature matrix definitions as separate download options. RNA data at https://doi.org/10.5281/zenodo.7041848 and ATAC data at https://doi.org/10.5281/zenodo.7058381. Dataset access details: AdamsonWeissman2016[7]: GSE90546 on GEO[55]; AissaBenevolenskaya2021[68]: GSE149383 on GEO; ChangYe2021[69]: E-MTAB-10698 on ArrayExpress[70]; DatlingerBock2017[1]: GSE92872 on GEO; DatlingerBock2021[71]: GSE168620 on GEO; DixitRegev2016[2]: GSE90063 on GEO; FrangiehIzar2021[6]: SCP1064 on the Broad Single Cell Portal https://singlecell.broadinstitute.org/single_cell/study/SCP1064/multi-modal-pooled-perturb-cite-seq-screens-in-patient-models-define-novel-mechanisms-of-cancer-immune-evasion; GasperiniShendure2019[54]: GSE120861 on GEO; GehringPachter2019[19]: https://doi.org/10.22002/D1.1311 on CaltechDATA; LiscovitchBrauerSanjana2021[59]: GSE161002 on GEO; McFarlandTsherniak2020[72]: https://doi.org/10.6084/m9.figshare.5863776.v1 on figshare; MimitouSmibert2021[73]: GSE156476 on GEO; NormanWeissman2019[49]: GSE133344 on GEO; PapalexiSatija202[9]: GSE153056 on GEO; PierceGreenleaf2021[42]: data deposited on AWS, URIs to be found at https://www.ncbi.nlm.nih.gov/pmc/articles/PMC8137922/bin/41467_2021_23213_MOESM9_ESM.xlsx; ReplogleWeissman2022[20]: processed single-cell data from gwps.wi.mit.edu; SchiebingerLander2019[23]: GSE106340 and GSE115943 on GEO; SchraivogelSteinmetz2020[74]: GSE135497 on GEO; ShifrutMarson2018[75]: GSE119450 on GEO; SrivatsanTrapnell2020[52]: GSE139944 on GEO; TianKampmann2019[76]: GSE152988 on GEO with mappings from kampmannlab.ucsf.edu/crop-seq; TianKampmann2021[21]: GSE124703 on GEO; WeinrebKlein2020[77]: GSE140802 on GEO; XieHon2017[78]: GSE81884 on GEO; ZhaoSims2021[79]: GSE148842 on GEO.

Code availability

Open access source code is at https://github.com/sanderlab/scPerturb/. We compiled a corresponding Python package called `scperturb` for performing E-statistics (E-distance and E-testing) in single-cell data, published on PyPI under https://pypi.org/project/scperturb/. Access details for the original publication for each dataset are available in the scPerturb GitHub repository (https://github.com/sanderlab/scPerturb) in the subfolder 'dataset_processing'.

References

60. Vierstra, J. et al. Global reference mapping of human transcription factor footprints. *Nature* **583**, 729–736 (2020).
61. Satpathy, A. T. et al. Massively parallel single-cell chromatin landscapes of human immune cell development and intratumoral T cell exhaustion. *Nat. Biotechnol.* **37**, 925–936 (2019).
62. Wolf, F. A., Angerer, P. & Theis, F. J. SCANPY: large-scale single-cell gene expression data analysis. *Genome Biol.* **19**, 15 (2018).
63. Bairoch, A. The Cellosaurus, a cell-line knowledge resource. *J. Biomol. Tech.* **29**, 25–38 (2018).
64. Mölder, F. et al. Sustainable data analysis with Snakemake. *F1000Res.* **10**, 33 (2021).
65. Rizzo, M. L. & Székely, G. J. Energy distance. *WIREs Comput. Stat.* **8**, 27–38 (2016).

66. Dhapola, P. et al. Scarf enables a highly memory-efficient analysis of large-scale single-cell genomics data. *Nat. Commun.* **13**, 4616 (2022).
67. Love, M. I., Huber, W. & Anders, S. Moderated estimation of fold change and dispersion for RNA-seq data with DESeq2. *Genome Biol.* **15**, 550 (2014).

References

70. Parkinson, H. et al. ArrayExpress: a public database of microarray experiments and gene expression profiles. *Nucleic Acids Res.* **35**, D747–D750 (2007).

Acknowledgements

The authors appreciate informative conversations with Y. Ji of the Fabian Theis laboratory, helpful code suggestions from G. Wong, and computational support from A. Kollasch of the Debora Marks laboratory. The authors also appreciate preprint review comments from Arcadia Science's preprint review initiative (G. P. Way, N. Davidson, E. Serrano, P. Hicks, J. Tomkinson, D. Bunten). This work was supported by the National Resource for Network Biology (NRNB, P41GM103504 to C.Sa.), the Wellcome Leap ΔTissue Program (to C.Sa., L.J.S., D.S.M.), the Deutsche Forschungsgemeinschaft (DFG, RTG2424 CompCancer to N.B.), Einstein Stiftung Berlin (Einstein Visiting Fellow program, to C.Sa., N.B.), and the Intramural Research Program of the National Library of Medicine, National Institutes of Health (to A.L.). Computation was in part performed on the HPC for Research cluster of the Berlin Institute of Health. Figures 1 and 4b were created with BioRender.com.

Author contributions

The project was conceptualized by C.Sa., N.B., A.L. and B.Y. Data were curated by T.D.G., S.P., C.Sh., T.G. and S.G. Formal analysis and methodology development were carried out by S.P., T.D.G. and C.Sa. Funding acquisition was done by N.B., D.S.M., L.J.S. and C.Sa. Software development was carried out by J.M., S.P. and T.D.G. Supervision was provided by N.B., A.L., J.P.T.-K., C.Sa., D.S.M. and L.J.S. The original draft was written by T.D.G., S.P., C.Sh., T.G. and J.P.T.-K. Writing review and editing were done by L.J.S., C.Sa., N.B. and A.L.

Competing interests

J.P.T.-K. and T.G. are employees of Relation Therapeutics. C.Sa. is on the science advisory board of Cytoreason Ltd. D.S.M. serves as an advisor for Dyno Therapeutics, Octant, Jura Bio, Tectonic Therapeutic, and Genentech, and is a co-founder of Seismic Therapeutic. All other authors have no competing interests.

Additional information

Extended data are available for this paper at https://doi.org/10.1038/s41592-023-02144-y.

Supplementary information The online version contains supplementary material available at https://doi.org/10.1038/s41592-023-02144-y.

Correspondence and requests for materials should be addressed to Stefan Peidli, Augustin Luna, Nils Blüthgen or Chris Sander.

Peer review information *Nature Methods* thanks the anonymous reviewers for their contribution to the peer review of this work. Peer reviewer reports are available. Primary Handling Editor: Lin Tang, in collaboration with the *Nature Methods* team.

https://doi.org/10.1038/s41592-023-02144-y

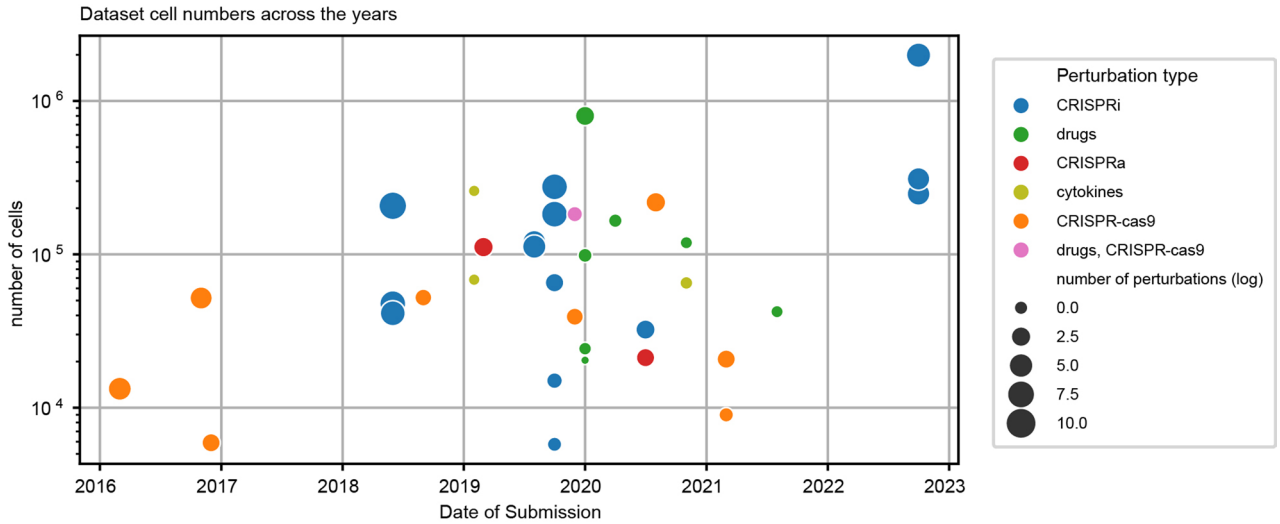

Extended Data Fig. 1 | Number of cells per dataset by submission date. There is a rapid increase in published single-cell perturbation datasets around 2019. We speculate that the slight decrease of dataset numbers after 2021 suggested by the plot is due to the ongoing impact of reduced research in the earlier phases of the COVID-19 pandemic.

https://doi.org/10.1038/s41592-023-02144-y

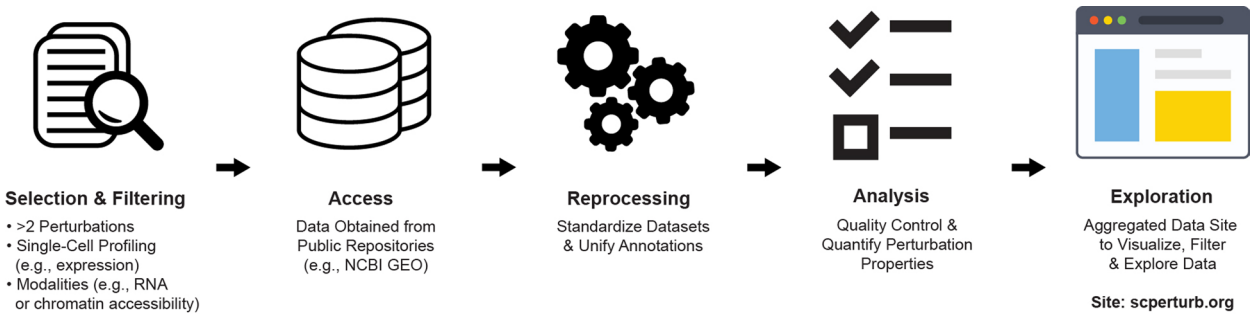

Extended Data Fig. 2 | Harmonization and analysis workflow. Perturbation datasets with single-cell molecular profiles with at least two perturbations and one control condition (for example unperturbed) of various modality types were identified in a literature search. Data were obtained from public repositories, and metadata (such as guide identity) from paper supplements. Datasets were reprocessed to standardize annotations and analyzed in parallel. All datasets are now available for download from scperturb.org, along with visualizations and summarizing information.

https://doi.org/10.1038/s41592-023-02144-y

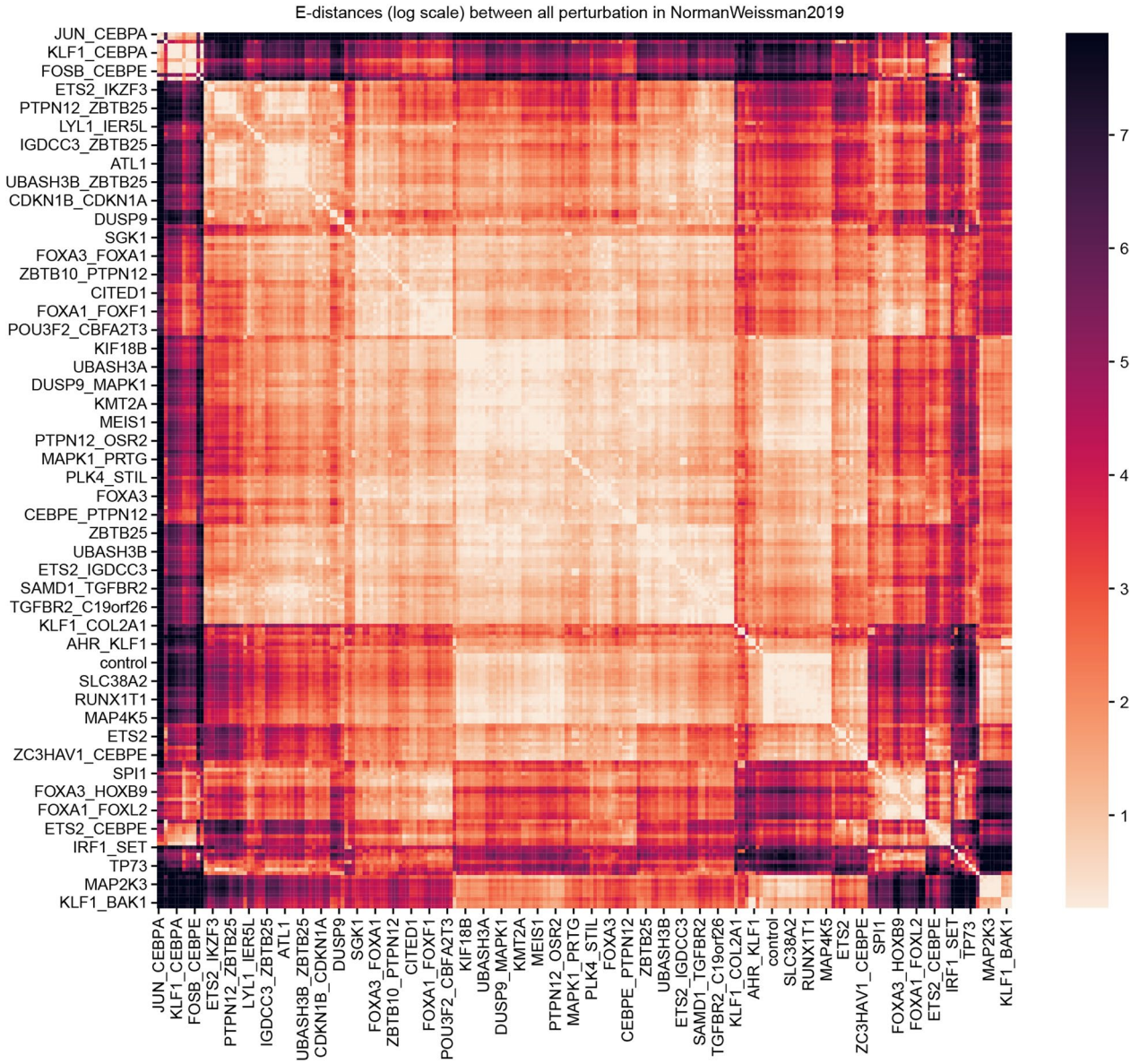

Extended Data Fig. 3 | Pairwise E-distances for NormanWeissman2019 dataset. E-distances between all pairs of perturbations in the dataset NormanWeissman2019. The color scale is clipped at 5% highest and lowest percentiles. Clusters of similar perturbations are visible, for example a cluster of strongly acting perturbations targeting CEBPA at the top.

nature portfolio

Corresponding author(s): Chris Sander, Nils Blüthgen, Augustin Luna, Stefan Peidli

Last updated by author(s): 9/15/2023

Reporting Summary

Nature Portfolio wishes to improve the reproducibility of the work that we publish. This form provides structure for consistency and transparency in reporting. For further information on Nature Portfolio policies, see our Editorial Policies and the Editorial Policy Checklist.

Statistics

For all statistical analyses, confirm that the following items are present in the figure legend, table legend, main text, or Methods section.

n/a	Confirmed
☐	☒ The exact sample size (*n*) for each experimental group/condition, given as a discrete number and unit of measurement
☒	☐ A statement on whether measurements were taken from distinct samples or whether the same sample was measured repeatedly
☐	☒ The statistical test(s) used AND whether they are one- or two-sided *Only common tests should be described solely by name; describe more complex techniques in the Methods section.*
☒	☐ A description of all covariates tested
☐	☒ A description of any assumptions or corrections, such as tests of normality and adjustment for multiple comparisons
☐	☒ A full description of the statistical parameters including central tendency (e.g. means) or other basic estimates (e.g. regression coefficient) AND variation (e.g. standard deviation) or associated estimates of uncertainty (e.g. confidence intervals)
☐	☒ For null hypothesis testing, the test statistic (e.g. *F*, *t*, *r*) with confidence intervals, effect sizes, degrees of freedom and *P* value noted *Give P values as exact values whenever suitable.*
☒	☐ For Bayesian analysis, information on the choice of priors and Markov chain Monte Carlo settings
☒	☐ For hierarchical and complex designs, identification of the appropriate level for tests and full reporting of outcomes
☐	☒ Estimates of effect sizes (e.g. Cohen's *d*, Pearson's *r*), indicating how they were calculated

Our web collection on statistics for biologists contains articles on many of the points above.

Software and code

Policy information about availability of computer code

Data collection	All data collection code is available on the associated git repo (https://github.com/sanderlab/scPerturb/), and as an archival version on Zenodo doi:10.5281/zenodo.8349131
Data analysis	Data analysis was performed in Python as described in the associated git repo (https://github.com/sanderlab/scPerturb/) and in the archival Zenodo repository doi:10.5281/zenodo.8349131. The file sc_env.yaml lists all packages that are required to replicate this analysis. Version numbers used here are: python 3.9, ArchR 1.0.1, scanpy versions 1.7.2–1.9.1 (uploaded AnnData objects were saved using 1.9.1), AnnData 0.9.1, h5py 3.9.0, igraph 0.10.6, leidenalg 0.10.1, libzlib 1.2.13, matplotlib 3.7.2., numba 0.57.1, numpy 1.24.4, pandas 2.0.3, scikit-learn 1.3.0, scikit-misc 0.3.0, scipy 1.11.2, sparse 0.14.0, umap-learn 0.5.3

For manuscripts utilizing custom algorithms or software that are central to the research but not yet described in published literature, software must be made available to editors and reviewers. We strongly encourage code deposition in a community repository (e.g. GitHub). See the Nature Portfolio guidelines for submitting code & software for further information.

Data

Policy information about availability of data

All manuscripts must include a data availability statement. This statement should provide the following information, where applicable:

- Accession codes, unique identifiers, or web links for publicly available datasets
- A description of any restrictions on data availability
- For clinical datasets or third party data, please ensure that the statement adheres to our policy

The website scperturb.org stores harmonized datasets with the following:
● scRNA-seq and antibody-based protein datasets: .h5ad files.
● scATAC-seq: multiple different feature matrix definitions as separate download options.

● RNA data at https://zenodo.org/record/7041849 and ATAC data at https://zenodo.org/record/7058382
● Dataset access details:
o AdamsonWeissman20167: GSE90546 on GEO(Barrett et al., 2013).
o AissaBenevolenskaya202157: GSE149383 on GEO.
o ChangYe202158: E-MTAB-10698 on ArrayExpress(Parkinson et al., 2007)
o DatlingerBock20171: GSE92872 on GEO.
o DatlingerBock202159: GSE168620 on GEO.
o DixitRegev20162: GSE90063 on GEO.
o FrangiehIzar20216: SCP1064 on the Broad Single Cell Portal https://singlecell.broadinstitute.org/single_cell/study/SCP1064/multi-modal-pooled-perturb-cite-seq-screens-in-patient-models-define-novel-mechanisms-of-cancer-immune-evasion
o GasperiniShendure201954: GSE120861 on GEO.
o GehringPachter201919: https://doi.org/10.22002/D1.1311 on CaltechDATA.
o Liscovitch-BrauerSanjana202160: GSE161002 on GEO
o McFarlandTsherniak202061: https://doi.org/10.6084/m9.figshare.5863776.v1 on figshare
o MimitouSmibert202162: GSE156476 on GEO
o NormanWeissman201949: GSE133344 on GEO.
o PapalexiSatija20219: GSE153056 on GEO.
o PierceGreenleaf202142: data deposited on AWS, URIs to be found at https://www.ncbi.nlm.nih.gov/pmc/articles/PMC8137922/bin/41467_2021_23213_MOESM9_ESM.xlsx
o ReplogleWeissman202220: processed single cell data from gwps.wi.mit.edu
o SchiebingerLander201923: GSE106340 and GSE115943 on GEO.
o SchraivogelSteinmetz202063: GSE135497 on GEO.
o ShifrutMarson201864: GSE119450 on GEO.
o SrivatsanTrapnell202052: GSE139944 on GEO.
o TianKampmann201965: GSE152988 on GEO with mappings from kampmannlab.ucsf.edu/crop-seq
o TianKampmann202121: GSE124703 on GEO
o WeinrebKlein202066: GSE140802 on GEO
o XieHon201767: GSE81884 on GEO
o ZhaoSims202168: GSE148842 on GEO

Human research participants

Policy information about studies involving human research participants and Sex and Gender in Research.

Reporting on sex and gender	N/A
Population characteristics	N/A
Recruitment	N/A
Ethics oversight	N/A

Note that full information on the approval of the study protocol must also be provided in the manuscript.

Field-specific reporting

Please select the one below that is the best fit for your research. If you are not sure, read the appropriate sections before making your selection.

☒ Life sciences ☐ Behavioural & social sciences ☐ Ecological, evolutionary & environmental sciences

For a reference copy of the document with all sections, see nature.com/documents/nr-reporting-summary-flat.pdf

Life sciences study design

All studies must disclose on these points even when the disclosure is negative.

Sample size	The manuscript describes an analysis method and data collection. We had no influence on determining the sample size of the data that is used in the study. We studied the influence of sample size on E-statistics (see Fig 5). Based off these results, in other portions of the paper we subset to all conditions with at least 200 cells, and randomly sampled cells from each perturbation condition.
Data exclusions	The manuscript describes an analysis method and data collection. We had no influence on determining excluded data from the original studies. When data was subset prior to analysis, we subset to all conditions with at least 200 cells, and randomly sampled cells from each perturbation condition. In the non-perturbation analysis in Section 8 of the Supplemental Note all conditions were subset to 91 cells per cell type in the full dataset analysis, and were not subset in the individual donor analysis.
Replication	The manuscript describes an analysis method and data collection. We had no influence on determining the replication of the data that is used in the study.
Randomization	The manuscript describes an analysis method and data collection. We had no influence on determining the randomization of the data that is used in the study.
Blinding	The manuscript describes an analysis method and data collection. We had no influence on determining the blinding of the data that is used in the study.

Reporting for specific materials, systems and methods

We require information from authors about some types of materials, experimental systems and methods used in many studies. Here, indicate whether each material, system or method listed is relevant to your study. If you are not sure if a list item applies to your research, read the appropriate section before selecting a response.

Materials & experimental systems

n/a	Involved in the study
☒	☐ Antibodies
☒	☐ Eukaryotic cell lines
☒	☐ Palaeontology and archaeology
☒	☐ Animals and other organisms
☒	☐ Clinical data
☒	☐ Dual use research of concern

Methods

n/a	Involved in the study
☒	☐ ChIP-seq
☒	☐ Flow cytometry
☒	☐ MRI-based neuroimaging